

See discussions, stats, and author profiles for this publication at: <https://www.researchgate.net/publication/256607454>

Spherical Monovalent Ions at Aqueous Liquid–Vapor Interfaces: Interfacial Stability and Induced Interface Fluctuations

ARTICLE *in* THE JOURNAL OF PHYSICAL CHEMISTRY B · SEPTEMBER 2013

Impact Factor: 3.3 · DOI: 10.1021/jp406001b · Source: PubMed

CITATIONS

6

READS

19

4 AUTHORS, INCLUDING:



Yuan Hu

University of Delaware

11 PUBLICATIONS 79 CITATIONS

SEE PROFILE



Sandeep A Patel

University of Delaware

72 PUBLICATIONS 1,765 CITATIONS

SEE PROFILE

Spherical Monovalent Ions at Aqueous Liquid–Vapor Interfaces: Interfacial Stability and Induced Interface Fluctuations

Shuching Ou, Yuan Hu, and Sandeep Patel*

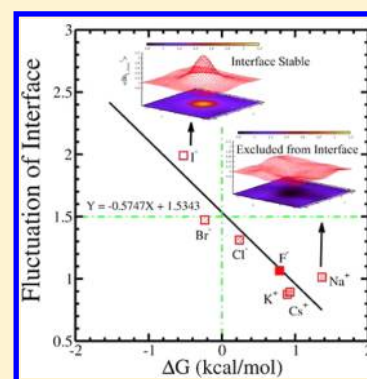
Department of Chemistry and Biochemistry, University of Delaware, Newark, Delaware 19716, United States

Hongbin Wan

Department of Chemical and Biomolecular Engineering, University of Delaware, Newark, Delaware 19716, United States

S Supporting Information

ABSTRACT: Ion-specific interfacial behaviors of monovalent halides impact processes such as protein denaturation, interfacial stability, and surface tension modulation, and as such, their molecular and thermodynamic underpinnings garner much attention. We use molecular dynamics simulations of monovalent anions in water to explore effects on distant interfaces. We observe long-ranged ion-induced perturbations of the aqueous environment, as suggested by experiment and theory. Surface stable ions, characterized as such by minima in potentials of mean force computed using umbrella sampling MD simulations, induce larger interfacial fluctuations compared to nonsurface active species, conferring more entropy approaching the interface. Smaller anions and cations show no interfacial potential of mean force minima. The difference is traced to hydration shell properties of the anions, and the coupling of these shells with distant solvent. The effects correlate with the positions of the anions in the Hofmeister series (acknowledging variations in force field ability to recapitulate essential underlying physics), suggesting how differences in induced, nonlocal perturbations of interfaces may be related to different specific-ion effects in dilute biophysical and nanomaterial systems.



1. INTRODUCTION

Molecular and atomic origins of the numerous physical effects induced by the addition of solutes and cosolutes to aqueous environments continue to garner tremendous scientific attention; in particular, questions about the driving forces for such processes, (free) energetic and entropic underpinnings of these effects, and general, quantitative models are actively pursued. A short list of relevant issues includes protein denaturation and folding in aqueous solutions by cosolutes,^{1,2} Hofmeister effects related to modulation of surface tension and protein solubility,^{3–5} anion-specific interfacial stability,^{6–10} as suggested by ambient pressure X-ray photoelectron spectroscopy (XPS), vibrational sum frequency generation (VSFG), and second-harmonic generation (SHG) studies of liquid–vapor (L–V) interfaces of aqueous halide solutions, and differential cation influences on multiwalled carbon nanomaterial aggregation kinetics.¹¹ In these contexts, the role of the interface, defined loosely as the boundary between water and any relevant (bio)molecular species, is critical. Moreover, the response of the water–(bio)molecule interface to added impurities would be central to such effects. Furthermore, one may ask about how the impurity might influence the behavior of the interface from afar? Is there a plausible interpretation? We bring to attention recent studies suggesting that ions modulate hydration water structure and properties over large distances;^{12–19} even large macromolecules have been shown to induce dramatically long-ranged perturbations of water

dynamics.²⁰ First hydration shell water molecules may not provide a complete picture in terms of understanding the above-mentioned physical behaviors in a holistic manner. Acknowledging long-range perturbations by impurities, one must connect such perturbations to observed physical phenomena. Here we attempt to provide a connection between local ion hydration, long-range perturbations, and surface stability of Hofmeister series anions, acknowledging that this is one specific context. In this work, we stress that we are not commenting on the accuracy of any of these force fields, as all water–ion force field combinations have been carefully parametrized and validated via extensive structural and thermodynamic analysis elsewhere. We are interested in extracting underlying behaviors that possibly help to discern between species exhibiting interfacial stability and those that do not. To achieve this, in the context of spherical, monovalent ion thermodynamics at aqueous L–V interfaces, we will apply classical molecular dynamics simulations using a set of different nonadditive and additive intermolecular potential functions to compute the reversible work of moving an ion from bulk to vapor through the interface; we will also extract from these all-atom simulation fluctuations of the L–V interface and, specifically, the manner in which the ions and their complex

Received: June 17, 2013

Revised: July 30, 2013

Published: July 31, 2013



hydration shells couple with solvent to give rise to interfacial fluctuations. The connection between differences in induced interface fluctuations and differences in solvation environment of a series of monovalent ions is a novel finding of this work. In section IIA we will discuss the methods, force fields, and other analysis protocols. In section IIC, we briefly present our analysis of instantaneous interfaces and their fluctuations as extracted from all-atom molecular dynamics simulations (following a method developed by Willard and Chandler²¹), and in section III we will present our results of potentials of mean force for a variety of ions modeled with polarizable and nonpolarizable force fields, interface fluctuations, and how each ion affects these, and finally connecting the nature of hydration shells of the series of ions to the trends in surface/interface stability demonstrated by the potentials of mean force.

II. METHODS

A. Simulation Details. In this study we used one nonpolarizable force field as well as three different polarizable force fields. We will first introduce the common simulation protocol, then describe them in detail. Molecular dynamics simulations were performed using the CHARMM package²² (for SPC/E, TIP4P-FQ, and TIP4P-QDP) and the parallel, scalable MD program NAMD 2.9b3²³ (for SWM4-NDP). Simulations of L-V interfaces were performed in the *NVT* ensemble. Temperature was maintained at $T = 300$ K using Nosé-Hoover thermostat²⁴ for SPC/E, TIP4P-FQ, and TIP4P-QDP, while Langevin friction force scheme was used in NAMD with the damping coefficient = 5 ps^{-1} for SWM4-NDP. The simulation cell was rectangular with dimensions $24 \text{ Å} \times 24 \text{ Å} \times 100 \text{ Å}$, in which z is the direction normal to the L-V interface. Periodic boundary conditions were applied in all three spatial directions. A bulk slab consisting of 988 water molecules (represented by the nonpolarizable SPC/E model²⁵ as well as the polarizable TIP4P-FQ model,²⁶ TIP4P-QDP,^{27,28} or SWM4-NDP²⁹) and a single ion (F^- , Cl^- , Br^- , I^- , Na^+ , K^+ , Cs^+) was positioned in the center of the simulation cell, resulting in two L-V interfaces (Table 1). A rigid water geometry is enforced using SHAKE³⁰ constraints. Before the production simulations, the system of each window was equilibrated for at least 0.5 ns.

Table 1. Parameters of Water Models Used in This Study

	R_{min} (Å)	ϵ (kcal/mol)
SPC/E	3.5532	0.1554
TIP4P-FQ	3.5459	0.2862
SWM4-NDP	3.5698	0.2057
TIP4P-QDP	3.5520	0.2902

1. TIP4P-FQ and TIP4P-QDP. We employ polarizable TIP4P-FQ²⁶ and TIP4P-QDP^{28,31} water models and nonpolarizable ions treated as charged Lennard-Jones spheres. Polarization of water is treated with a charge equilibration Hamiltonian:^{32–35}

$$E_{\text{elec}} = \sum_{i=1}^N (\chi_i) q_i + \frac{1}{2} \sum_{i=1}^N \eta_i q_i^2 + \frac{1}{2} \sum_{i \neq j}^N J_{ij} q_i q_j \quad (1)$$

where χ_i and η_i may be associated with atomic electronegativities and hardnesses, respectively; the J_{ij} terms represent a parametrized molecular Coulomb integral between pairs of atoms. Components of the molecular polarizability tensor are related to the inverse of the hardness matrix (constructed from

the values of η_i and J_{ij} above) as $\alpha_{\beta\gamma} = \mathbf{R}_\beta \mathbf{J}^{-1} \mathbf{R}_\gamma$, where \mathbf{R}_β represents the β Cartesian components of the atomic position vector.³⁶

Both water models employ a rigid geometry having an O–H bond distance of 0.9572 Å, an H–O–H bond angle of 104.52° and a massless, off-atom M site located 0.15 Å along the H–O–H bisector, which carries the oxygen partial charge. Repulsion and dispersion interactions are modeled using a single Lennard-Jones (LJ) site located on the oxygen center having parameters $R_{\text{min,O}} = 3.5459 \text{ Å}$ and $\epsilon_{\text{O}} = 0.2862 \text{ kcal mol}^{-1}$ for TIP4P-FQ, $R_{\text{min,O}} = 3.5606 \text{ Å}$ and $\epsilon_{\text{O}} = 0.3501 \text{ kcal mol}^{-1}$, respectively.

Ions were treated as nonpolarizable particles with interaction parameters based on those by Lamoureux and Roux³⁷ and validated for use with TIP4P-FQ.^{38–42} For ions in TIP4P-QDP, the parameters were obtained from ref 42. Ion parameters in SPC/E were parametrized by Fyta et al.^{43,44} We acknowledge that the use of a mixed polarizable water model with nonpolarizable anion representation may appear unorthodox, but we consider that the combination of this *empirical* model is well-validated and reproduces many of the currently accepted experimental observables upon which the quality of such force fields are based. Furthermore, the use of an alternative force field model allows us to speak to the universality (or at least the broad commonality) of molecular and atomic features underlying observed behaviors such as surface stability and negative surface adsorption entropy.

We summarize the parameters used in Table 2. The nonbond interactions were treated via the standard Lennard-Jones “12–6” potential

$$E_{\text{LJ}} = \sum_{ij} \epsilon_{ij} \left(\frac{R_{\text{min},ij}^{12}}{r_{ij}^{12}} - 2 \frac{R_{\text{min},ij}^6}{r_{ij}^6} \right) \quad (2)$$

Lennard-Jones interactions were gradually switched off at interparticle distance of 11 Å, with a gradual switching between 10 and 11 Å using the switching function:

$$S(r_{ij}) = \begin{cases} 1 & r_{ij} \leq r_{\text{on}} \\ \frac{(r_{\text{off}}^2 - r_{ij}^2)^2 (r_{\text{off}}^2 + 2r_{ij}^2 - 3r_{\text{on}}^2)}{(r_{\text{off}}^2 - r_{\text{on}}^2)^3} & r_{\text{on}} < r_{ij} \leq r_{\text{off}} \\ 0 & r_{ij} > r_{\text{off}} \end{cases} \quad (3)$$

Charge degrees of freedom for the TIP4P-FQ and TIP4P-QDP water models were coupled to a thermostat at 1 K with a mass of $0.000069 \text{ kcal mol}^{-1} \text{ ps}^2 \text{ e}^{-2}$ using the Nosé-Hoover method, and the charge degrees of freedom were propagated in an extended Lagrangian formalism; each water molecule was taken as a charge normalization unit (charge conserved with this unit), thus, preventing any charge transfer between water molecules or between water and ion. We acknowledge recent developments of charge transfer models of water^{45,46} and anticipate that application of charge transfer models to the study of specific-ion effects will soon be realized and further elucidate underlying mechanisms and physics. Conditionally convergent long-range electrostatic interactions were treated using a Particle Mesh Ewald (PME)⁴⁷ approach with a $30 \times 30 \times 128$ point grid, sixth order interpolation, and $\kappa = 0.33$. Dynamics were propagated using a Verlet leapfrog integrator with a 0.5 fs time step for TIP4P-FQ and TIP4P-QDP, 1 fs

Table 2. Parameters of Ions Used in This Study^a

	R_{\min} (Å)	ϵ (kcal/mol)	ΔG_{hyd} (kcal/mol)
SPC/E			
F [−]	4.6706	0.003585	−102.77
Cl [−]	4.9388	0.1	−73.14
Br [−]	5.1981	0.09847	−66.68
I [−]	6.5451	0.003085	−57.60
Na ⁺	2.8993	0.1	−98.95
K ⁺	3.0194	0.5832	−82.22
Cs ⁺	3.9185	0.07768	−71.22
TIP4P-FQ			
F [−]	4.52	0.01	−112.83(9)
Cl [−]	4.92	0.07658	−78.93(8)
Br [−]	5.14	0.10820	−71.87(14)
I [−]	5.52	0.15910	−63.15(15)
Na ⁺	2.90	0.03151	−98.41(12)
K ⁺	3.29	0.18290	−82.05(10)
Cs ⁺	3.96	0.35279	−69.63(8)
SWM4-NDP			
F [−]	4.9245	0.002618	−108.0
Cl [−]	4.9622	0.07197	−78.4
Br [−]	5.2526	0.0823	−71.6
I [−]	5.5159	0.2084	−63.1
Na ⁺	2.9234	0.0315	−96.3
K ⁺	3.3733	0.1419	−78.6
TIP4P-QDP			
Cl [−]	5.6419	0.01142	−74.4(2)
Br [−]	5.6839	0.05740	−63.1(7)
I [−]	5.8339	0.1569	−57.5(1)
Na ⁺	2.6939	0.031075	−103.2(1)

^aUncertainty in the last digit denoted in parentheses.

time step for SPC/E. Total sampling time for each window was 5–20 ns; properties were calculated from all but the initial 0.5 ns, which was treated as equilibration.

2. SWM4-NDP. Associated with the explicit SWM4-NDP water force field, ions were also represented with a Drude oscillator model as discussed in ref 48. The parameters were obtained from ref 48. A time step of 1.0 fs was used to integrate the equations of motion. Particle Mesh Ewald (PME) was implemented to treat conditionally convergent long-range electrostatic interactions (using a grid of $32 \times 32 \times 128$ points). The cutoff for van der Waals (VDW) interactions was set to 15 Å without smoothing functions. An analytical correction of Lennard-Jones was applied to the reported VDW energy and virial that is equal to the amount lost due to cutoff of the LJ potential. The temperature was kept constant by applying the Langevin friction force scheme (5 ps^{-1} was used for the damping coefficient).

The long-range Coulombic forces were updated every two steps. The VDW interactions were modified using scale 1–3 parameters defined in the NAMD protocol and truncated smoothly at the cutoff distance. To ensure near-SCF conditions, the thermostat for the relative motion of the Drude particles with respect to their parent atoms was set at a temperature of 1 K with a damping coefficient of 20 ps^{-1} . The rigid geometry of the SWM4-NDP water molecule was maintained using the SETTLE algorithm.⁴⁹ An additional quartic restraining potential of $4000 \text{ kcal/mol/Å}^2$, fitted from QM calculations, was applied to a Drude oscillator if its length exceeded 0.2 Å (fitted from QM calculations). These technical details are implemented in NAMD2.9 and were used without

modification in the current work. A NAMD input file for the Drude oscillator ABF simulation for sodium cation in SWM4-NDP water is provided at the end of the Supporting Information.

B. Potential of Mean Force Calculation. We will present potential of mean force (PMF) results for the reversible work of transferring ions from bulk solution through the L-V interface, to the vapor phase. The PMF will characterize the interfacial stability of each ion. Computational experiments measuring the reversible work (potential of mean force, PMF) for transferring single ions/molecules from bulk aqueous environment to the aqueous solution L-V interface have enjoyed a long history as a means to explore the origins of surface stability.^{50–52} For potential of mean force calculations of SPC/E, TIP4P-FQ, and TIP4P-QDP, our reaction coordinate, ξ_0 , is the Cartesian z-component of the separation between the water slab center of mass and ion center of mass. In all simulations used for computing potentials of mean force, ions were restrained to z-positions from 10 to 35 Å relative to the water slab center of mass using a harmonic potential $U_{\text{restraint}}(z; z_{\text{relative,ref}}) = (1/2)k_{\text{restraint}}(z - z_{\text{relative,ref}})^2$ with the force constant of 4 (kcal/mol)/Å²; this encompasses a range approximately 15 Å below the Gibbs Dividing Surface (GDS) to approximately 10 Å above it at 300 K; though one could probe separations further into the bulk (toward the center of the system), this distance is sufficient to probe the differences of interest in this study and also in keeping with previous studies to which we compare our results. We note the recent connection of the potential of mean force to thermodynamic free energies:⁵³

$$\frac{dA(\xi_0)}{d\xi_0} = \left\langle \left(\frac{\partial U_{\text{interaction}}(r^N)}{\partial q_\xi} \right)_{\{q_{m \neq \xi}\}^{N-1}} \right\rangle_{\xi_0} - \left\langle \frac{1}{\beta} \left(\frac{\partial \ln |J|}{\partial \xi} \right)_{\{q_{m \neq \xi}\}^{N-1}} \right\rangle_{\xi_0} - \frac{1}{\beta} \left\langle \sum_{m \neq \xi}^{N-1} \left[\delta(q_m - l_{U_m}) \frac{dl_{U_m}(q_m)}{dq_\xi} - \delta(q_m - l_{L_m}) \frac{dl_{L_m}(q_m)}{dq_\xi} \right] \right\rangle_{\xi_0} \quad (4)$$

where the interaction potential is taken to be a function of some set, of the size of the number of system degrees of freedom, of generalized coordinates, q_ξ . The reaction coordinate of interest in this case corresponds to $q_\xi = \xi_0$. The first term is the negative of the mean force whose integral over the domain of the reaction coordinate yields the potential of mean force. The second term arises from the volume scaling upon transforming from Cartesian to some generalized curvilinear space (represented in general by the set of generalized coordinates). The last term arises from interchange of the order of the differential and integral operators according to Leibniz rule. In the present study, as we retain the Cartesian z-component of the separation between centers of mass (the force is projected along this reaction coordinate), and the domain of the reaction coordinate is decoupled from those of the remaining coordinates (the derivatives in the Leibniz term

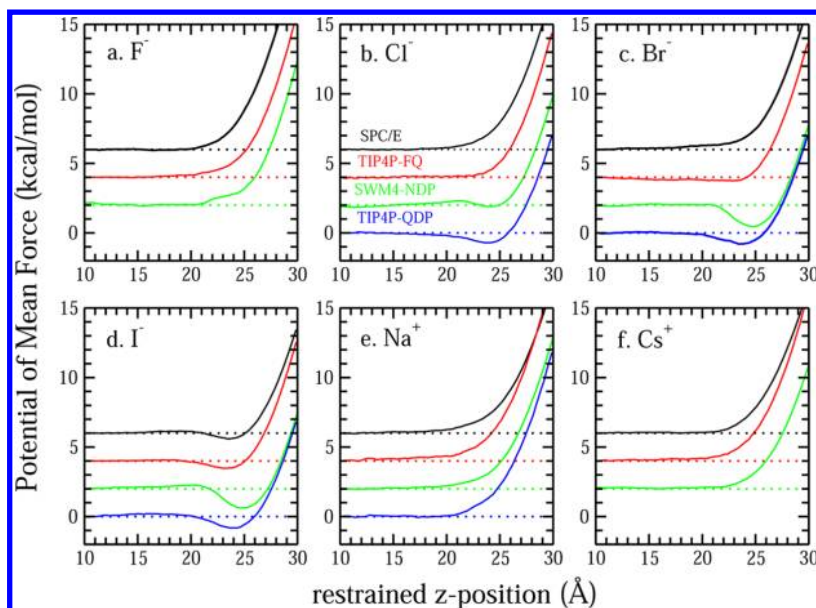


Figure 1. Potential of mean force for single ions transporting from bulk to vapor phase in different water force fields. A vertical offset of 2 kcal/mol is added for clarity.

are zero), the Jacobian and Leibniz terms vanish. Thus, we discuss the PMF in terms of the free energy or reversible work for the remainder of the paper.

The free energy profiles in SWM4-NDP force field were performed by using NAMD software with the Adaptive Biasing Force (ABF) extensions integrated in the Collective Variables module and under the same conditions as described for MD simulations. A total of 32 “windows” along the positive z -direction were explored, each with 1.5 Å width. Force samples were accumulated in bins 0.02 Å $[-1.5-00.5]$, $[00-01.5]$, $[01-02.5]$, $[02-03.5]$, $[03-04.5]$, $[04-05.5]$, $[05-06.5]$, $[06-07.5]$, $[07-08.5]$, $[08-09.5]$, $[09-10.5]$, $[10-11.5]$, $[11-12.5]$, $[12-13.5]$, $[13-14.5]$, $[14-15.5]$, $[15-16.5]$, $[16-17.5]$, $[17-18.5]$, $[18-19.5]$, $[19-20.5]$, $[20-21.5]$, $[21-22.5]$, $[22-23.5]$, $[23-24.5]$, $[24-25.5]$, $[25-26.5]$, $[26-27.5]$, $[27-28.5]$, $[28-29.5]$, $[29-30.5]$, $[30-31.5]$.

The uncertainties in potentials of mean force are determined using the approach of Zhu and Hummer:⁵⁴

$$\text{var}[G(\xi_N)] \approx \sum_{i=1}^N \text{var}[K\Delta\xi\bar{z}_i] \quad (5)$$

where \bar{z}_i is the mean position of z in the i_{th} window, which can be obtained from block averages.⁵⁵ K is the force constant. The corresponding standard deviation $\sigma[G(\xi_N)]$ is then the square root of $\text{var}[G(\xi_N)]$. In our case, $G(z_{\text{bulk}}) = 0$; therefore, the last window is expected to have the largest uncertainty. The largest uncertainties for the systems are approximately 0.1 kcal/mol (shown in Figure 1 of Supporting Information). Alternative measures of estimating the mean and uncertainty of other properties will be discussed as needed.

C. Instantaneous Interfaces and Surface Fluctuations.

For an instantaneous surface snapshot, the local density profile can be defined as⁵⁶

$$\langle \rho(\vec{r}_{xy}, z) \rangle \equiv \frac{1}{A_\xi} \int d^2\vec{r}'_{xy} \rho(\vec{r}_{xy} - \vec{r}'_{xy}, z) = \rho[z - h(\vec{r}_{xy})] \quad (6)$$

which describes the short-distance average of the density over an area $A_\xi \sim \xi^2$ at position \vec{r}_{xy} . ξ is an inherent correlation length. Here we define $\delta h(\vec{r}_{xy}) = h(\vec{r}_{xy}) - z$ as surface height function. Notice that under this definition we have $\langle \delta h(\vec{r}_{xy}) \rangle = 0$.

From individual snapshot/configuration we can construct the coarse-grained instantaneous surface defined by Willard and Chandler.⁵⁷ Gaussian mass distributions are assigned to each water oxygen atom:

$$\Phi(\mathbf{r}; \xi) = (2\pi\xi^2)^{-d/2} \exp(-r^2/2\xi^2) \quad (7)$$

where r is the magnitude of \mathbf{r} , ξ is taken as 3.0 Å, and d stands for dimensionality (3 in this case). At space-time point \mathbf{r} , t , we have the coarse-grained density as

$$\bar{\rho}(\mathbf{r}, t) = \sum_j \Phi(|\mathbf{r} - \mathbf{r}_j(t)|; \xi) \quad (8)$$

The interface is then determined as the $(d - 1)$ dimensional manifold with a constant value c . In practice, we set up series of spacial grid points (x, y, z) and compute the corresponding coarse-grained densities $\rho(x, y, z)$ by eq 8.⁵⁸ The resolution we use for x and y dimensions is 0.6 Å between grid points; for z dimension the grid resolution is 0.1 Å. The surface is then obtained as the manifold by setting $\rho(x, y, z) = \rho_{\text{bulk}}/2$. With sufficient sampling, we can average these instantaneous surfaces $(h_t(x, y))$, at time t and get the mean surface $\langle h(x, y) \rangle$; furthermore, $\langle \delta h(x, y) \rangle = 0$. Subtracting the mean values from the $h_t(x, y)$, we obtain $\delta h_t(x, y)$ and the height fluctuations $\delta h_t^2(x, y)$. Using this framework to characterize interface fluctuations, we can probe the magnitudes of interface fluctuations when the ions reside at various positions along the reaction coordinate.

III. RESULTS AND DISCUSSION

A. Potential of Mean Force and Surface Fluctuation.

We begin by looking at the free energetics of ions across the L-V interface. This will show which of the model ions (in their respective types of solvent) are predicted to be interface stable

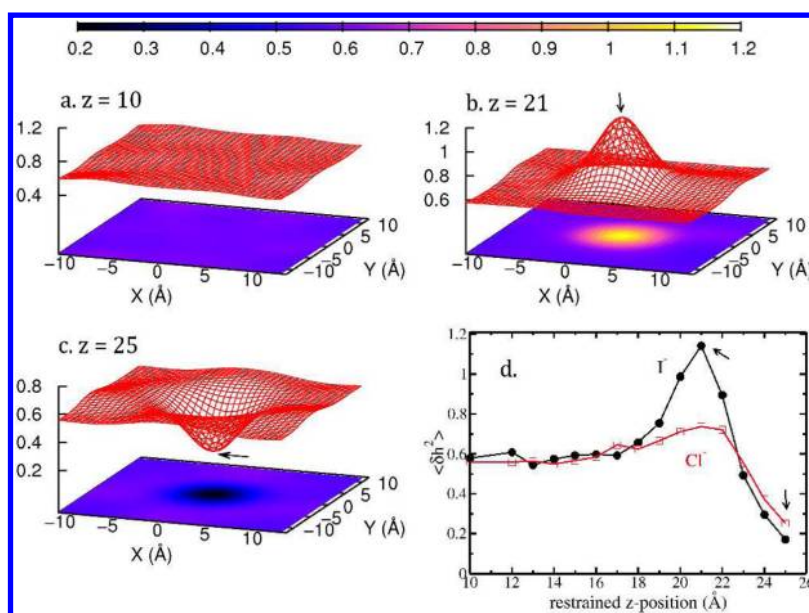


Figure 2. Average surface fluctuation $\langle \delta h^2 \rangle$ for I^- in TIP4P-FQ, when the restrained position is at (a) $z = 10$ Å, (b) $z = 21$ Å, and (c) $z = 25$ Å. (d) $\langle \delta h^2(x = 0, y = 0) \rangle$ (right above/below the ion, as indicated with arrows) as a function of ion restrained position for I^- and Cl^- in TIP4P-FQ.

and to what extent as indicated by the magnitude of the PMF well-depth at the interface. In all cases, the position of the Gibbs dividing surface (GDS) is around $z = 25.6$ Å; because the GDS is determined predominantly by the water density, the presence of a single ion of varying size does not influence to any large extent the less-resolved GDS across all systems. Figure 1 shows the potential of mean force (PMF) of single anion/cation in different force fields (K^+ is shown in Figure 2 of Supporting Information). For clarity, we added a vertical offset of 2 kcal/mol between each force field. As a reminder, for SPC/E, TIP4P-FQ, and TIP4P-QDP, we used umbrella sampling in conjunction with WHAM⁵⁹ to compute the PMF; for SWM4-NDP, we used ABF. The PMF is defined to be zero in the bulk (which is determined by window $z = 10$ Å). The PMF from ABF method is consistent with the umbrella sampling method, which is verified in Supporting Information, Figure 11. All the cations and F^- shows no PMF minimum regardless of force field. For Cl^- , the TIP4P-QDP force field shows modest surface stability; in SWM4-NDP, there is a barrier observed around $z = 21$ Å, followed by a shallow minimum after the barrier. We observed PMF minima for Br^- in polarizable force fields but no surface stability in nonpolarizable force fields. Br^- has been considered marginally surface stable so the greatest effect of polarization may be expected to occur with this ion (i.e., surface stability systematically emerging with the introduction of ion polarizability). For I^- , PMF minima are observed in all force fields with the sequence $\Delta G_{\text{SWM4-NDP}} < \Delta G_{\text{TIP4P-QDP}} < \Delta G_{\text{TIP4P-FQ}} \approx \Delta G_{\text{SPC/E}}$. The results for Drude I^- are consistent with the surface stability discussed by Archontis et al.⁶⁰ Incidentally, at 300 K, I^- shows a minimum of 0.5 kcal/mol in TIP4P-FQ, which is similar to the result for iodide at the L-V interface using nonpolarizable ions in SPC/E water by Horinek et al.^{61,62} This also corresponds with the DFT-D value determined by Baer et al.,⁶³ though we do not discount that ours is a fortuitous result to some degree. In our simulation, we do not include explicitly the polarization of the I^- , but we have taken care to faithfully capture the relative hydration free energetics of the individual ions to as great an extent as possible. Though not possible currently, it would be interesting

to connect the hydration free energetics of ions using DFT-D methods in order to further assess and characterize such agreements between classical models and electron-density based models.

Recent studies have demonstrated a connection between L-V interfacial stability of chemical species (i.e., a free energy minimum state with the solute at the interface) and the extent to which the presence of these molecular species in the vicinity of the interface induces collective fluctuations of the interface in addition to the level inherent in pure water due to thermal motion.^{6,58} In the next discussion, we explore the differences in interfacial fluctuations for the various ions discussed in this study. We aim to further demonstrate the general connection between interfacial stability and fluctuations with different force fields.

Figure 2 shows the fluctuations $\langle \delta h^2(x, y) \rangle$ for I^- at different restrained z -position in TIP4P-FQ force field. When the anion is in the bulk (i.e., $z = 10$ Å), $\langle \delta h^2(x, y) \rangle$ is about 0.56, which corresponds to the value of pure TIP4P-FQ (refer to ref 58); at $z = 18.0$ Å, we observe onset of enhanced fluctuations relative to the pure water system. This enhancement reaches a maximum, while I^- is restrained at $z = 21$ Å (as shown in Figure 2b). Finally, when the anion moves across the GDS ($z = 25$ Å), the interfacial fluctuation is suppressed (as shown in Figure 2c). To illustrate this feature, we plot $\langle \delta h^2(x = 0, y = 0) \rangle$ as a function of the anion restrained z -position, as presented in Figure 2d.

From Figure 2b,c we can see that the geometry of the $\langle \delta h^2(x, y) \rangle$ surface possesses radial symmetry and can thus be presented as a function of the lateral distance $r = (x^2 + y^2)^{1/2}$. In the case of pure water (in the absence of ions), $\langle \delta h^2 \rangle$ for the current system size for the current force fields are 0.62 (SPC/E), 0.56 (TIP4P-FQ), 0.52 (SWM4-NDP), and 0.58 (TIP4P-QDP). Therefore, in order to demonstrate and compare the fluctuations induced from the ions, we define $\delta h_L^2(r)$ as the fluctuations normalized by the value of pure water fluctuation in the corresponding force field. In this convention, when $\langle \delta h_L^2 \rangle$ equals 1, the effect of ion is zero; when $\langle \delta h_L^2 \rangle > 1$, the surface height fluctuation is enhanced relative to pure water with the

presence of ion; when $\langle \delta h_L^2 \rangle < 1$, the surface height fluctuation is suppressed. Here we would like to address that, although the surface fluctuation of pure water for the same force field does change according to the size of the simulation cell (basically, the larger the x, y dimensions, the larger the fluctuation value), the normalized $\langle \delta h_L^2 \rangle$ remains the same for the same ion at the same relative position along the reaction coordinate, which indicates that the ion-induced fluctuation is indeed a characteristic of the ion and is system size independent (data shown in Supporting Information, Figure 4).

Figure 3 shows the $\langle \delta h_L^2(r) \rangle$ from I^- (surface stable in all force fields) and Na^+ (nonsurface stable), at the restrained

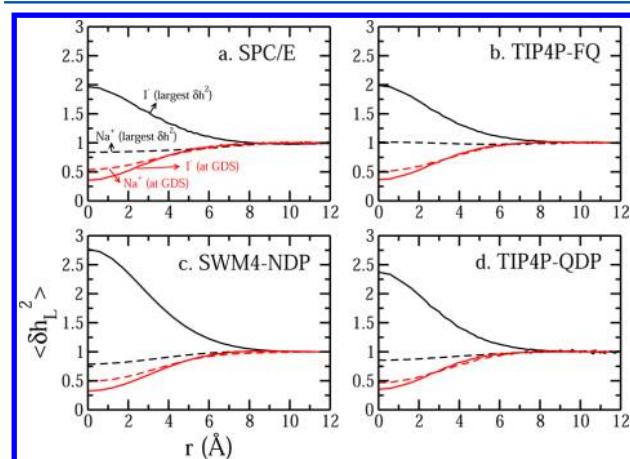


Figure 3. Normalized average surface fluctuation $\langle \delta h_L^2 \rangle$ as a function of radius from the I^-/Na^+ in (a) SPC/E, (b) TIP4P-FQ, (c) SWM4-NDP, and (d) TIP4P-QDP force fields.

window which induces the largest possible surface fluctuation and GDS. Fluctuation profiles for other ions can be found in Supporting Information, Figures 5–10). Here we chose these two species to describe the general properties and connection between surface stability and surface height fluctuation. First, either anion or cation suppresses the fluctuation when the ion is at the GDS, which is consistent with previous studies.^{6,58,64} Na^+ does not generate any fluctuation enhancement. Only the surface stable species, I^- , induces interfacial fluctuation, in fact, up to two times the inherent fluctuation from pure water. This fluctuation enhancement can influence the interface up to 8 Å from the ion center. Furthermore, at $r = 0$ Å (which indicates right above/below the ion), we have $\langle \delta h_{L,\text{SWM4-NDP}}^2 \rangle > \langle \delta h_{L,\text{TIP4P-QDP}}^2 \rangle > \langle \delta h_{L,\text{TIP4P-FQ}}^2 \rangle > \approx \langle \delta h_{L,\text{SPC/E}}^2 \rangle$. This is the opposite sequence of the corresponding ΔG values. We also notice that, from Figure 2d, which plots values of $\langle \delta h_L^2(r=0) \rangle$ as a function of ion position along the interface normal from bulk to GDS (and Figure 7 of ref⁵⁸), though Cl^- in TIP4P-FQ induces less enhancement of fluctuations (about half of I^- -induced), yet we still find no surface stability for Cl^- in TIP4P-FQ water. This suggests a threshold level of induced fluctuations separating surface-stable ions; this would be ion-specific and the precise value for a particular ion–water force field would be determined by the complex interplay of water–water, ion–water interactions, and how these vary with proximity to the ion (i.e., nature of hydration shell of the ion in a particular solvent force field model as we will discuss further below). Furthermore, we have demonstrated that, for species such as Cl^- in TIP4P-FQ water, there is no temperature-dependent variation of $\langle \delta h_L^2(r) \rangle$, opposite to

what is observed for I^- ; we interpret this to mean that there is no real interfacial enhancement from the non-surface-stable ion. This is rationalized by the fact that with increasing temperature, the increased inherent thermal fluctuations of the water interface wash out any induced fluctuations arising from perturbation of solvent structure by the ion.⁵⁸

To summarize up to this point, we have found that, across a variety of force fields for ions and solvent, there is a group of ions that exhibit interfacial stability as seen in the potentials of mean force. In this work, we stress that we are not commenting on the accuracy of any of these force fields, as all water–ion force field combinations have been carefully parametrized and validated via extensive structural and thermodynamic analysis elsewhere. We have then seen that the species demonstrating an interfacial stability appear to enhance L-V interfacial fluctuations significantly, while those that show no interfacial stability induce no further fluctuation (or may even suppress levels of fluctuations). Our analysis further suggests the existence of inherent levels of fluctuation that correspond to interfacial stability that are force field specific and arise from complex interactions of the models. Figure 4 shows results of

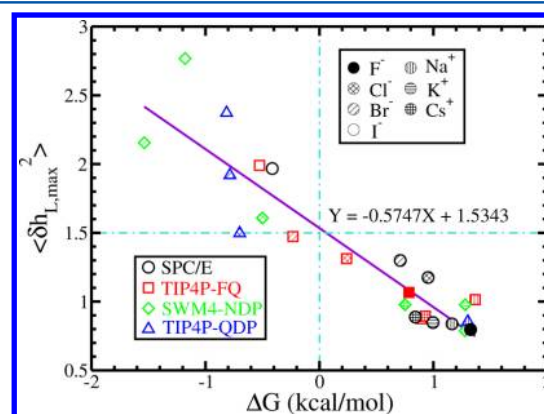


Figure 4. Largest normalized average surface fluctuation $\langle \delta h_{L,\text{max}}^2 \rangle$ vs. the corresponding free energy ΔG for ions in different force fields. All cations, which are not found to be surface stable in our work, are located in the lower right quadrant of the graph. All surface stable species (anions described by certain force fields) are found in the upper left quadrant.

the PMF value at the position of the GDS versus the maximum interfacial fluctuations induced. This is a plot that only distinguishes between ions; the different water force fields are not isolated. We see that the ions displaying interface stability lie in the upper left quadrant of the figure; those showing no stability (positive values of PMF) reside in the lower right quadrant. A best-fit straight line indicates a threshold value of about 1.5 dividing those ions that are interfacially stable and those that are not. The value of 1.5 is not an absolute threshold; this will depend on the force field (as noted above) and size of the interfacial area and is sensitive to the parameters of the protocol (width of Gaussian for coarse-graining water density) used to compute instantaneous interfaces and fluctuations. Nevertheless, the qualitative behavior and results should be robust.

We will next attempt to explain the current observations by considering the interaction of the local hydration environment of the ions with the solvent and solvent fluctuations at the L-V interface. We aim to show that the two types of ions (surface stable and unstable) present distinct hydration shell environ-

ments toward the interface upon approach; the surface stable ions presenting a solvent environment that is less rigid, more malleable, and thus, more amenable to inducing fluctuations of the interface as a consequence of a greater disruption of solvent structure on approach to the interface. The non-surface-stable ions present a more rigid hydration environment due to the more effective hydrogen bonding of water, thus, decreasing the efficacy of promoting interfacial fluctuations. These properties of the two orientations are discussed using radial density profiles of water around the single ions and water velocity autocorrelation functions in the hydration shells presented to the interface in the vicinity of the GDS.

B. Solvation Structure and Dynamical Properties. We first consider general characteristics of ion hydration through radial density functions (RDFs) shown in Figure 5. In panels a–

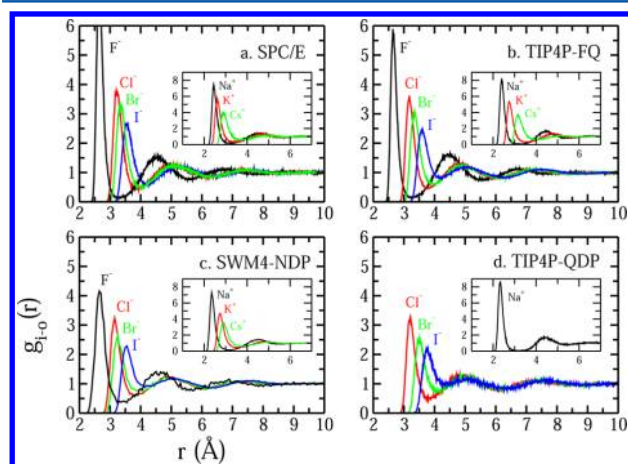


Figure 5. Ion–water radial distribution function (RDF) for anions in (a) SPC/E, (b) TIP4P-FQ, (c) SWM4-NDP, and (d) TIP4P-QDP force fields. The insets show the RDF of cations in the corresponding force field.

d we show results for anions and cations (in insets) in the various water models (on F^- ion model has been developed for the TIP4P-QDP water force field currently). Regardless of water force field or inclusion of polarizability, there is a general trend from F^- to I^- of decreasing water structuring around the anion (similarly for the cation series from Na^+ to Cs^+). The more severe ordering of water molecules around Cl^- is well-known.^{65,66} Smaller anions show dramatic first solvation peaks and a sharply oscillatory probability function; in contrast, the larger anions show modest peaks, and significantly less oscillations. Figure 6a–c shows the 360° angle-averaged radial water density around I^- , Cl^- , and Na^+ as they reside at $z = 21.0$ Å, the position of maximum $\langle \delta h_s^2(x, y) \rangle$ for the anions (the cation shows no maximum, but we use the same distance for all ions for consistency). This figure demonstrates the different manners in which the hydration shells of the ions couple with the solvent at the interface. I^- , while retaining its first, weakly bound, less-ordered (malleable) hydration shell, sheds its outer hydration layers in the sense that these shells intermingle with the interfacial solvent. Cl^- , in contrast, retains the first and most of the second hydration shells (two bright rings); thus, the hydration shell environment is more rigid, well-ordered, tightly bound to the ion and does not support increased dynamical perturbation of local solvent. Moving to the cation, Na^+ , panel c demonstrates the unambiguous, well-defined hydration shells, with a fully intact second shell clearly visible. We conjecture

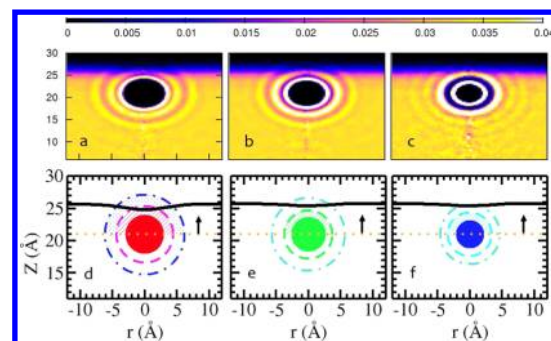


Figure 6. Average water oxygen density relative to (a) I^- , (b) Cl^- , and (c) Na^+ at the position of 21.0 Å. (d–f) Cartoon of ion with the cutoff of first solvation shell (dashed lines), second solvation shell (dot-dashed lines), and the calculated mean surface (solid black lines). For dynamical properties of water molecules in the shells of ions, we only study the water above the ion position (dotted lines).

that the differences in water dynamics and structure in the first and second hydration shells of I^- and Cl^- lead to differences in induced interfacial fluctuations. To explore this, we will consider first water (oxygen) velocity autocorrelation functions (vacfs) and residence times of water in the hydration shells of select ions. Since our contention is based on the nature of the hydration shell environment presented to the interface as the ion approaches, we will consider properties of hydrating water above the ion as depicted in Figure 6d–f. Shown in panels d, e, and f are the mean coarse-grained interfaces when the ions are positioned at $z = 21$ Å. These panels further demonstrate how the hydration shells of each ion (boundaries of which are delineated by the dashed circles around each ion) interact with the mean interface and the interfacial region in general. In the case of I^- , it is plausible to entertain the idea that less ordered, dynamic, weakly bound water in these shells can help induced fluctuations about the mean interface. In the case of the other two ions, the mean interface is further away, and the rigidity of these ions' solvation shells prevents fluctuations that would penetrate into the local hydration shells. We now consider vacfs.

C. Water Velocity Autocorrelation Functions and Residence Times. Ensemble-averaged oxygen velocity autocorrelation functions (VACF),^{67–69}

$$C_v(t) = \frac{\langle \vec{v}_i(t) \cdot \vec{v}_i(0) \rangle}{\langle \vec{v}_i(0) \cdot \vec{v}_i(0) \rangle} \quad (9)$$

where $\vec{v}_i(t)$ is the velocity vector of the atom (the oxygen in our case) in i_{th} water molecule in the simulation system at time t . The brackets denote the ensemble average. Here we only look at the VACF of water oxygen above the ion and within the first/second shell.

Figure 7 shows oxygen–oxygen VACF for I^- and Cl^- in TIP4P-FQ water for three ion positions corresponding to bulk solution ($z = 10$ Å), position of maximum fluctuation enhancement ($z = 21$ Å), and the GDS ($z = 25$ Å). Autocorrelation functions are shown for first hydration shell waters (solid line), second hydration shell waters (dashed line), pure bulk water (open circles), and pure water L–V interface (open squares). The solid and dashed lines represent correlation functions for water molecules in the regions depicted in Figure 6. We see that the location of the ions influences the dynamics of water in their hydration shells. At the bulk, $z = 10$ Å, position, for both anions, autocorrelation

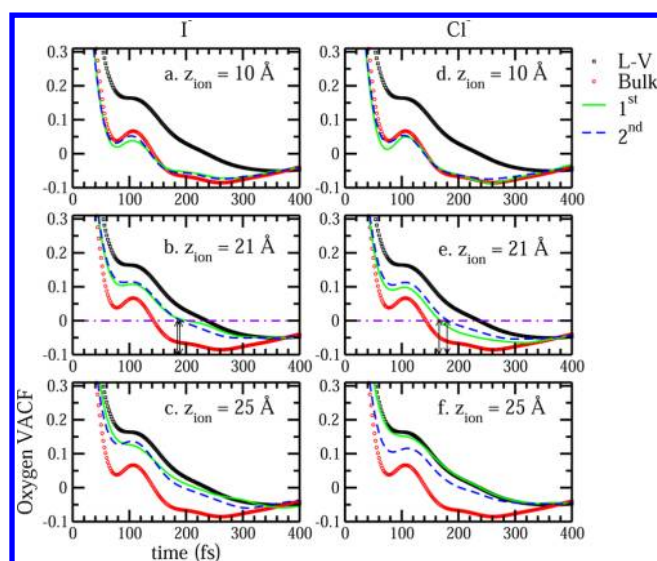


Figure 7. Oxygen velocity autocorrelation of water (TIP4P-FQ) in the bulk, near L-V interface, solvation shell water above I^-/Cl^- .

functions are bulk-like as expected. We notice the canonical caging effect of local solvent molecules manifest in oscillations around 100 fs. At ion position $z = 21$ Å, for the I^- system, we see little difference between autocorrelation decay in the first and second hydration shells unlike in the Cl^- system. The shortest time to approach zero is 185–190 fs for I^- , 160 fs for Cl^- in the first shell, and 180 ps for Cl^- in the second shell. The shorter decorrelation times for Cl^- are consistent with a higher shell water density. Furthermore, the I^- curve takes a form closer to that of the pure L-V interface, while the Cl^- curve retains the oscillatory “hump” (though damped) of the bulk liquid curve, particularly the Cl^- first hydration shell. This indicates that the well-known caging effect persists for Cl^- . The local hydration environments for I^- and Cl^- are quite different approaching the interface.

Water residence time is considered a time-dependent probability function $P(t)$ of a molecule uninterruptedly remaining in a region at time $t = t_0 + \Delta t$ having started in the region at time $t = 0$ $P(t) = (1/N(0)\sum_{t_0} N(t_0, t))$. We consider molecules that are within the first/second shell at time $t_0 = 0$ and remain within the corresponding shell at t with no instances of leaving the region. The probability is $P(t) = (1/N(0)\sum_{t_0} N(t_0, t))$

$$P(t) = \frac{1}{N(0)} \sum_{t_0} N(t_0, t) \quad (10)$$

where t_0 indicates multiple time origins and $t = t_0 + \Delta t$ is the persistence time of a water molecule in a region after it was initially observed at time origin t_0 . The number of molecules confined at each time t is normalized by the number of molecules observed at $t = 0$, such that $P(0) = 1$. We employ a 5 fs saving frequency for this analysis. $P(t)$ is fit to a stretched exponential, $P(t) = P_0 \exp[-(t/\tau)^\gamma]$

$$P(t) = P_0 \exp[-(t/\tau)^\gamma] \quad (11)$$

where P_0 , τ , and γ are adjustable fitting parameters. P_0 is the probability that a water molecule initially is within the shell at time $t = 0$; for the final functional fits, P_0 is approximately 1. γ is the well-known stretched exponential constant and is generally around 0.85, suggesting deviation from first order decay. τ is

characteristic residence lifetime. Residence times of water molecules (only those above the ion) residing in the first solvation of I^- and Cl^- are shown in Table 3. Data for I^- and

Table 3. Fitting Results of Residence Time of Water Molecules in the First Solvation Shell^a

system	τ (ps)	γ
I^- , TIP4P-FQ, 10.0 Å	1.62(0.28)	0.78(0.04)
I^- , TIP4P-FQ, 21.0 Å	1.12(0.25)	0.80(0.05)
I^- , TIP4P-FQ, 25.0 Å	1.47(0.13)	0.86(0.08)
Cl^- , TIP4P-FQ, 10.0 Å	2.57(0.22)	0.84(0.04)
Cl^- , TIP4P-FQ, 21.0 Å	2.74(0.08)	0.86(0.09)
Cl^- , TIP4P-FQ, 25.0 Å	2.46(0.08)	0.85(0.16)
I^- , SWM4-NDP, 10.0 Å	1.82(0.94)	0.76(0.14)
I^- , SWM4-NDP, 21.0 Å	1.27(0.86)	0.72(0.12)
I^- , SWM4-NDP, 25.0 Å	0.83(0.67)	1.04(0.25)
Cl^- , SWM4-NDP, 10.0 Å	3.38(1.91)	0.88(0.15)
Cl^- , SWM4-NDP, 21.0 Å	2.00(0.82)	0.91(0.10)
Cl^- , SWM4-NDP, 25.0 Å	2.41(2.33)	1.04(0.25)

^aValues in parentheses denote the uncertainty determined from the standard deviation.

Cl^- using TIP4P-FQ and SWM4-NDP water models are shown as representative examples. For all positions, water residence times in the first hydration shell of Cl^- are higher than for I^- . At $z = 21.0$ Å, the ratio can reach a striking factor of 2. This suggests that the first hydration shell of Cl^- acts as a barrier to surface deformation, preventing deformation to the extent observed for I^- ; moreover, the mean surface for Cl^- resides in its second hydration shell. Observed differences in ion-induced interfacial fluctuations thus correlate with the lifetimes of hydration water molecules in a particular ion's local environment, the implication being that faster dynamics (smaller lifetimes) allow more exchange of water in hydration shells, allowing for the ability to accommodate/mediate greater fluctuations.

IV. SUMMARY AND CONCLUSIONS

Our findings indicate a connection between interface stability and induced interfacial fluctuations for a series of anions and cations modeled using molecular dynamics simulations. The behavior, as summarized in Figure 4, appears to span a variety of force fields and does not discriminate based on inclusion or exclusion of polarization in the force field. For purposes of discussion and to connect to implications of this work for underlying mechanistic explanations of differential anion stability at aqueous L-V interfaces, or action of protein denaturing osmolytes, we explore semiquantitatively the relation between interface fluctuations and surface entropy. We stress that the surface/interfacial entropy is just one contribution to the overall system entropy. From the interface height function covariance matrix, $\chi(\mathbf{r}_i, \mathbf{r}_j) = \langle \delta h(\mathbf{r}_i) \delta h(\mathbf{r}_j) \rangle$, with $\delta h(\mathbf{r}_i) = h(\mathbf{r}_i) - \langle h(\mathbf{r}_i) \rangle$, multivariate statistics gives the entropy as $S = \text{constant} + (1/2)k_B \ln|\chi|$ (refer to Supporting Information). Figure 8 (symbols) shows estimates of the resulting interfacial entropy (relative to ion z -position 10.0 Å) at ion positions of 21.0 and 25.0 Å; we stress that these values are qualitative due to the grid-based approach used. In the barrier region, the entropy from surface fluctuations increases for both ions, with I^- contributing more due to larger fluctuations. We posit that in the case of I^- , this higher interfacial entropy acts in conjunction with other enthalpic (i.e.,

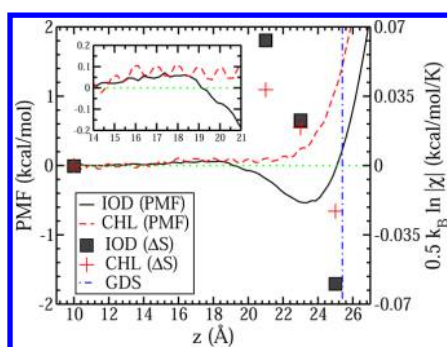


Figure 8. Potentials of mean force (PMF's) for I^- and Cl^- in TIP4P-FQ. Inset shows the region of ion positions from $z = 14.0$ to 21.0 Å. Symbols are semiquantitative estimates of surface entropy (relative to bulk, hence ΔS) arising from ion-induced interfacial fluctuations using $S = \text{constant} + (k_B/2) \ln |\chi|$, where χ is the surface height function covariance matrix whose elements are $\chi(\mathbf{r}_i, \mathbf{r}_j) = \langle \delta h(\mathbf{r}_i) \delta h(\mathbf{r}_j) \rangle$. Finally, $\delta h(\mathbf{r}_i) = h(\mathbf{r}_i) - \langle h(\mathbf{r}_i) \rangle$.

increase in water–water interactions leading to enthalpic stabilization of the system) contributions to greater stabilize I^- at these locations ($z = 20.0, 21.0$, and 22.0 Å) compared to Cl^- . This translates to higher probability of the I^- being in these positions; once at these locations, the I^- can then proceed to the interfacial region. At the Gibbs Dividing Surface (vertical line, Figure 8), suppression of interface fluctuations by both anions leads to lower surface entropy relative to the bulk state. In the case of I^- , the reduction is slightly higher consistent with the trends in Figure 1. The surface adsorbed state for I^- shows a net decrease in entropy relative to the bulk state; this holds for Cl^- as well. For I^- , this is interpreted as one negative contribution to the standard entropy of adsorption.

In summary, negatively charged ionic impurities, I^- and Cl^- , induce long-ranged solvent perturbations that propagate to an interface when the ions are up to 8 Å away in accord with recent experiments and interpretations suggesting the long-range nature of ion-induced perturbations. Furthermore, we observe chemical specificity (ion-specificity); I^- induces larger interfacial fluctuations than Cl^- . The differences in induced fluctuations are traceable to the nature of the first few hydration shells of the ions. For I^- , the hydration shells consist of water molecules that are more dynamic, less persistent (lower residence times), while the opposite is true for Cl^- . Approaching the L-V interface, coupling of local solvent with solvent further away leads to differential contributions of surface entropy (arising from the different magnitudes of the interface fluctuations) to the stability of surface-adsorbed states. Long-range perturbations are not only relevant to the bulk, but also to the nature of fluctuations at water-biomacromolecule and water-nanomaterial interfaces.

Addressing implications of this work, we note the striking similarity of hydration properties of the less charge-dense I^- to that of hydrophobic hydration.⁷⁰ Analogous to enhanced solvent density fluctuations seen for molecular hydrophobic solutes in water,⁷⁰ I^- perturbs solvent structure and dynamics (to a greater degree than Cl^-) leading to more fluid, dynamic, and fluctuating solvent structure. Furthermore, our observation regarding the connection between the extent of “rigidity” of the first hydration shell of the impurity and its surface stability is reminiscent of Figure S2 of the Supporting Information of ref 6. Overall, results indicate that ion-specific surface adsorption of

inorganic monovalent anions may be discussed in the context of increasing ion hydrophobic character as recently suggested.^{62,71}

■ ASSOCIATED CONTENT

Supporting Information

Fluctuation profiles for all ions studied in this work. Further details of entropy calculations are also provided. Comparison of PMF's obtained using umbrella sampling with WHAM and Adaptive Biasing Force method are shown. Uncertainty in PMF calculations are also discussed. Sample input script for NAMD calculation is also provided. This material is available free of charge via the Internet at <http://pubs.acs.org>.

■ AUTHOR INFORMATION

Corresponding Author

*E-mail: sapatel@udel.edu.

Notes

The authors declare no competing financial interest.

■ ACKNOWLEDGMENTS

The authors acknowledge partial support from the National Institutes of Health (COBRE:SP20RR017716-07) at the University of Delaware, Department of Chemistry and Biochemistry. Computational resources are acknowledged via support from National Institutes of Health (COBRE:P20-RR015588) in the Chemical Engineering Department at the University of Delaware. This work is also partially supported by National Science Foundation CAREER AWARD (MCB-1149802) to S.P. We thank Professor Phillip Geissler and Patrick Shaffer for sharing code for analysis of interface fluctuations and resulting entropy. We acknowledge N. Patel for fruitful discussions and guidance throughout this work.

■ REFERENCES

- (1) Hua, L.; Zhou, R.; Thirumalai, D.; Berne, B. J. Urea Denaturation by Stronger Dispersion Interactions with Proteins than Water Implies a 2-Stage Unfolding. *Proc. Natl. Acad. Sci. U.S.A.* **2008**, *105*, 16928–16933.
- (2) Beauchamp, K. A.; McGibbon, R.; Lin, Y.-S.; Pande, V. S. Simple Few-State Models Reveal Hidden Complexity in Protein Folding. *Proc. Natl. Acad. Sci. U.S.A.* **2012**, *109*, 17807–17813.
- (3) Hofmeister, F. About Regularities in the Protein Precipitating Effects of Salts and the Relation of These Effects with the Physiological Behavior of Salts. *Arch. Expt. Pathol. Pharmacol.* **1887**, *24*, 247–260.
- (4) Baldwin, R. L. How Hofmeister Ion Interactions Affect Protein Stability. *Biophys. J.* **1996**, *71*, 2056–2063.
- (5) Pegram, L. M.; Wendorff, T.; Erdmann, R.; Shkel, I.; Bellissimo, D.; Felitsky, D. J.; Record, M. T. Why Hofmeister Effects of Many Salts Favor Protein Folding But Not DNA Helix Formation. *Proc. Natl. Acad. Sci. U.S.A.* **2010**, *107*, 7716–7721.
- (6) Otten, D. E.; Shaffer, P. R.; Geissler, P. L.; Saykally, R. J. Elucidating the Mechanism of Selective Ion Adsorption to the Liquid Water Surface. *Proc. Natl. Acad. Sci. U.S.A.* **2012**, *109*, 701–705.
- (7) Noah-Vanhoeck, J.; Geissler, P. L. On the Fluctuations That Drive Small Ions Towards and Away From Interfaces Between Polar Liquids and Their Vapors. *Proc. Natl. Acad. Sci. U.S.A.* **2009**, *106*, 15125–15130.
- (8) Ghosal, S.; Brown, M. A.; Bluhm, H.; Krisch, M. J.; Salmeron, M.; Jungwirth, P.; Hemminger, J. C. Ion Partitioning at the Liquid/Vapor Interface of a Multi-component Alkali Halide Solution: A Model for Aqueous Sea Salt Aerosols. *J. Phys. Chem. A* **2008**, *112*, 12378–12384.
- (9) Ghosal, S.; Hemminger, J. C.; Bluhm, H.; Mun, B. S.; Hebenstreit, E. L. D.; Ketteler, G.; Ogletree, D. F.; Requejo, F. G.; Salmeron, M. Electron Spectroscopy of Aqueous Solution Interfaces Reveals Surface Enhancement of Halides. *Science* **2005**, *307*, 563–566.

- (10) Tobias, D.; Hemminger, J. C. Getting Specific About Specific Ion Effects. *Science* **2008**, *319*, 1197–1198.
- (11) Yi, P.; Chen, K. L. Influence of Surface Oxidation on the Aggregation and Deposition Kinetics of Multiwalled Carbon Nanotubes in Monovalent and Divalent Electrolytes. *Langmuir* **2012**, *27*, 3588–3599.
- (12) O'Brien, J. T.; Prell, J. S.; Bush, M. F.; Williams, E. R. Sulfate Ion Patterns Water at Long Distance. *J. Am. Chem. Soc.* **2010**, *132*, 8248–8249.
- (13) Tielrooij, K. J. Cooperativity in Ion Hydration. *Science* **2010**, *328*, 1006–1009.
- (14) Mancinelli, R.; Botti, A.; Bruni, F.; Ricci, M. A.; Soper, A. K. Perturbation of Water Structure Due to Monovalent Ions in Solution. *Phys. Chem. Chem. Phys.* **2007**, *9*, 2959–2967.
- (15) Horzmann, J.; Ludwig, R.; Geiger, A.; Paschek, D. Pressure and Salt Effects in Simulated Water: Two Sides of the Same Coin. *Angew. Chem., Int. Ed.* **2007**, *46*, 8907–8911.
- (16) Paschek, D.; Ludwig, R. Specific Ion Effects on Water Structure and Dynamics Beyond the First Hydration Shell. *Angew. Chem., Int. Ed.* **2011**, *50*, 352–353.
- (17) Galamba, N. Mapping Structural Perturbations of Water in Ionic Solutions. *J. Phys. Chem. B* **2012**, *116*, 5242–5250.
- (18) Botti, A.; Bruni, F.; Imberti, S.; Ricci, M. A.; Soper, A. K. Solvation Shell of H^+ Ions in Water. *J. Mol. Liq.* **2005**, *117*, 77–81.
- (19) Botti, A.; Bruni, F.; Imberti, S.; Ricci, M. A.; Soper, A. K. Solvation Shell of OH^- Ions in Water. *J. Mol. Liq.* **2005**, *117*, 81–84.
- (20) Born, B.; Kim, S. J.; Ebbinghaus, S.; Gruebele, M.; Havenith, M. The Terahertz Dance of Water with the Proteins: The Effect of Protein Flexibility on the Dynamical Hydration Shell of Ubiquitin. *Faraday Discuss.* **2009**, *141*, 161–173.
- (21) Willard, A. P.; Chandler, D. The Role of Solvent Fluctuations in Hydrophobic Assembly. *J. Phys. Chem. B* **2008**, *112*, 6187–6192.
- (22) Brooks, B. R.; Brooks, C. L.; MacKerell, A. D.; Nilsson, L.; Petrella, R. J.; Roux, B.; Won, Y.; Archontis, G.; Bartels, C.; Boresch, S. CHARMM: The Biomolecular Simulation Program. *J. Comput. Chem.* **2009**, *30*, 1545–1614.
- (23) Phillips, J. C.; Braun, R.; Wang, W.; Gumbart, J.; Tajkhorshid, E.; Villa, E.; Chipot, C.; Skeel, R. D.; Kale, L.; Schulten, K. Scalable Molecular Dynamics with NAMD. *J. Comput. Chem.* **2005**, *26*, 1781–1802.
- (24) Nosé, S. A Molecular Dynamics Methods for Simulations in the Canonical Ensemble. *Mol. Phys.* **1984**, *52*, 255–268.
- (25) Berendsen, H. J. C.; Grigera, J. R.; Straatsma, T. P. The Missing Term in Effective Pair Potentials. *J. Phys. Chem.* **1987**, *91*, 6269–6271.
- (26) Rick, S. W.; Stuart, S. J.; Berne, B. J. Dynamical Fluctuating Charge Force Fields: Application to Liquid Water. *J. Chem. Phys.* **1994**, *101*, 6141–6156.
- (27) Bauer, B. A.; Warren, G. L.; Patel, S. Incorporating Phase-Dependent Polarizability in Nonadditive Electrostatic Models for Molecular Dynamics Simulations of the Aqueous Liquid–Vapor Interface. *J. Chem. Theory Comput.* **2009**, *5*, 359–373.
- (28) Bauer, B. A.; Patel, S. Properties of Water Along the Liquid–Vapor Coexistence Curve via Molecular Dynamics Simulations Using the Polarizable TIP4P-QDP-LJ Water Model. *J. Chem. Phys.* **2009**, *131*, 084709.
- (29) Lamoureux, G.; Harder, E.; Vorobyov, I. V.; Roux, B.; MacKerell, A. D., Jr. Polarizable Model of Water for Molecular Dynamics Simulations of Biomolecules. *Chem. Phys. Lett.* **2006**, *418*, 245–249.
- (30) Ryckaert, J. P.; Ciccotti, G.; Berendsen, H. J. C. Numerical Integration of the Cartesian Equations of Motion of a System with Constraints: Molecular Dynamics of *n*-Alkanes. *J. Comput. Phys.* **1977**, *23*, 327–341.
- (31) Bauer, B. A.; Patel, S. Molecular Dynamics Simulations of Nonpolarizable Salt Solution Interfaces: NaCl, NaBr, and NaI in Transferable Intermolecular Potential 4-Point with Charge Dependent Polarizability TIP4P-QDP Water. *J. Chem. Phys.* **2010**, *132*, 8107–8117.
- (32) Sanderson, R. T. *Chemical Bonds and Bond Energy*; Academic Press: New York, 1976.
- (33) Rappe, A. K.; Goddard, W. A. Charge Equilibration for Molecular Dynamics Simulations. *J. Phys. Chem.* **1991**, *95*, 3358–3363.
- (34) Rick, S. W.; Stuart, S. J.; Bader, J. S.; Berne, B. J. Fluctuating Charge Force Fields for Aqueous Solutions. *J. Mol. Liq.* **1995**, *65/66*, 31.
- (35) Sanderson, R. T. An Interpretation of Bond Lengths and a Classification of Bonds. *Science* **1951**, *114*, 670–672.
- (36) Warren, G. L.; Davis, J. E.; Patel, S. Origin and Control of Superlinear Polarizability Scaling in Chemical Potential Equilization Methods. *J. Chem. Phys.* **2008**, *128*, 144110.
- (37) Lamoureux, G.; Roux, B. Absolute Hydration Free Energy Scale for Alkali and Halide Ions Established from Simulations with a Polarizable Force Field. *J. Phys. Chem. B* **2006**, *110*, 3308–3322.
- (38) Warren, G. L.; Patel, S. Hydration Free Energies of Monovalent Ions in Transferable Intermolecular Potential Four Point Fluctuating Charge Water: An Assessment of Simulation Methodology and Force Field Performance and Transferability. *J. Chem. Phys.* **2007**, *127*, 064509.
- (39) Warren, G. L.; Patel, S. Comparison of the Solvation Structure of Polarizable and Nonpolarizable Ions in Bulk Water and Near the Aqueous Liquid–Vapor Interface. *J. Phys. Chem. C* **2008**, *112*, 7455–7467.
- (40) Warren, G. L.; Patel, S. Electrostatic Properties of Aqueous Salt Solution Interfaces: A Comparison of Polarizable and Nonpolarizable Ion Models. *J. Phys. Chem. B* **2008**, *112*, 11679–11693.
- (41) Bauer, B. A.; Ou, S.; Patel, S. Role of Spatial Ionic Distribution on the Energetics of Hydrophobic Assembly and Properties of the Water/Hydrophobe Interface. *Phys. Chem. Chem. Phys.* **2012**, *14*, 1892–1906.
- (42) Bauer, B. A.; Ou, S.; Patel, S. Solvation Structure and Energetics of Single Ions at the Aqueous Liquid–Vapor Interface. *Chem. Phys. Lett.* **2011**, *527*, 22–26.
- (43) Fyta, M.; Kalcher, I.; Dzubiella, J.; Vrbka, L.; Netz, R. R. Ionic Force Field Optimization Based on Single-Ion and Ion-Pair Solvation Properties. *J. Chem. Phys.* **2010**, *132*, 024911.
- (44) Fyta, M.; Netz, R. R. Ionic Force Field Optimization Based on Single-Ion and Ion-Pair Solvation Properties: Going beyond Standard Mixing Rules. *J. Chem. Phys.* **2012**, *136*, 124103.
- (45) Wick, C. D.; Lee, A. J.; Rick, S. W. How Intermolecular Charge Transfer Influences the Air–Water Interface. *J. Chem. Phys.* **2012**, *137*, 154701.
- (46) Lee, A. J.; Rick, S. W. The Effects of Charge Transfer on the Properties of Liquid Water. *J. Chem. Phys.* **2011**, *134*, 184507.
- (47) Darden, T.; York, D.; Pedersen, L. Particle Mesh Ewald: An $N \log(N)$ Method for Ewald Sums in Large Systems. *J. Chem. Phys.* **1993**, *98*, 10089–10092.
- (48) Yu, H.; Whitfield, T. W.; Harder, E.; Lamoureux, G.; Vorobyov, I.; Anisimov, V. M.; MacKerell, A. D., Jr.; Roux, B. Simulating Monovalent and Divalent Ions in Aqueous Solution Using a Drude Polarizable Force Field. *J. Chem. Theory Comput.* **2010**, *6*, 774–786.
- (49) Miyamoto, S.; Kollman, P. A. Settle: An Analytical Version of the SHAKE and RATTLE Algorithm for Rigid Water Models. *J. Comput. Chem.* **1992**, *13*, 952–962.
- (50) Dang, L. X. Computational Study of Ion Binding to the Liquid Interface of Water. *J. Phys. Chem. B* **2002**, *106*, 10388–10394.
- (51) Wick, C. D.; Dang, L. X. Recent Advances in Understanding Transfer Ions across Aqueous Interfaces. *Chem. Phys. Lett.* **2008**, *458*, 1–5.
- (52) Dang, L. X.; Chang, T. M. Molecular Mechanism of Ion Binding to the Liquid/Vapor Interface of Water. *J. Phys. Chem. B* **2002**, *106*, 235–238.
- (53) Wong, K.-Y.; York, D. M. Exact Relation between Potential of Mean Force and Free-Energy Profile. *J. Chem. Theory Comput.* **2012**, *8*, 3998–4003.
- (54) Zhu, F.; Hummer, G. Convergence and Error Estimation in Free Energy Calculations Using the Weighted Histogram Analysis Method. *J. Comput. Chem.* **2012**, *33*, 453–465.

- (55) Flyvbjerg, H.; Petersen, H. G. Error Estimates on Averages of Correlated Data. *J. Chem. Phys.* **1989**, *91*, 461–466.
- (56) Pershan, P. S.; Schlossman, M. *Liquid Surfaces and Interfaces: Synchrotron X-ray Methods*; Cambridge University Press: Cambridge, 2012; p 4.
- (57) Willard, A. P.; Chandler, D. Instantaneous Liquid Interfaces. *J. Phys. Chem. B* **2010**, *114*, 1954–1958.
- (58) Ou, S.; Patel, S. Temperature Dependence and Energetics of Single Ions at the Aqueous Liquid–Vapor Interface. *J. Phys. Chem. B* **2013**, *117*, 6512–6523.
- (59) Kumar, S.; Bouzida, D.; Swendsen, R. H.; Kollman, P. A.; Rosenberg, J. M. The Weighted Histogram Analysis Method for Free-Energy Calculations on Biomolecules. I. The Method. *J. Comput. Chem.* **1992**, *13*, 1011–1021.
- (60) Archontis, G.; Leontidis, E.; Andreou, G. Attraction of Iodide Ions by Free Water Surface, Revealed by Simulations with a Polarizable Force Field Based on Drude Oscillators. *J. Phys. Chem. B* **2005**, *109*, 17957–17966.
- (61) Horinek, D.; Herz, A.; Vrbka, L.; Sedlmeier, F.; Mamatkulov, S. I.; Netz, R. R. Specific Ion Adsorption at the Air/Water Interface: The Role of Hydrophobic Solvation. *Chem. Phys. Lett.* **2009**, *479*, 173–183.
- (62) Netz, R. R.; Horinek, D. Progress in Modeling of Ion Effects at the Vapor/Water Interface. *Annu. Rev. Phys. Chem.* **2012**, *63*, 401–418.
- (63) Baer, M. D.; Mundy, C. J. Toward an Understanding of the Specific Ion Effect Using Density Functional Theory. *J. Phys. Chem. Lett.* **2011**, *2*, 1088–1093.
- (64) Stern, A. C.; Baer, M. D.; Mundy, C. J.; Tobias, D. J. Thermodynamics of Iodide Adsorption at the Instantaneous Air–Water Interface. *J. Chem. Phys.* **2013**, *138*, 114709.
- (65) Godec, A.; Smith, J. C.; Merzel, F. Increase of Both Order and Disorder in the First Hydration Shell with Increasing Solute Polarity. *Phys. Rev. Lett.* **2011**, *107* (267801), 1–5.
- (66) Lamoureux, G.; Roux, B. Absolute Hydration Free Energy Scale for Alkali and Halide Ions Established from Simulations with a Polarizable Force Field. *J. Phys. Chem. B* **2006**, *110*, 3308–3323.
- (67) Rahman, A. Correlations in the Motion of Atoms in Liquid Argon. *Phys. Rev.* **1964**, *136*, A405–A411.
- (68) Choudhury, N.; Pettitt, B. M. Dynamics of Water Trapped between Hydrophobic Solutes. *J. Phys. Chem. B* **2005**, *109*, 6422–6429.
- (69) Marti, J.; Nagy, G.; Guardia, E.; Gordillo, M. C. Molecular Dynamics Simulation of Liquid Water Confined inside Graphite Channels: Dielectric and Dynamical Properties. *J. Phys. Chem. B* **2006**, *110*, 23897–23994.
- (70) Jamadagni, S. N.; Godawat, R.; Garde, S. Hydrophobicity of Proteins and Interfaces: Insights from Density Fluctuations. *Ann. Rev. Chem. Biomol. Eng.* **2011**, *2*, 147–171.
- (71) Godec, A.; Merzel, F. Physical Origin Underlying the Entropy Loss upon Hydrophobic Hydration. *J. Am. Chem. Soc.* **2012**, *134*, 17574–17581.